Journal Pre-proofs

Probing fluconazole deposition inside mesoporous silica using solid-state NMR spectroscopy: crystallization of a confined metastable form and phase transformations under storage conditions

Maciej Nowak, Aleksandra J. Dyba, Anna M. Gołkowska, Aleksandra Nieckarz, Karolina Krajewska, Katarzyna Malec, Dinu Iuga, Bożena Karolewicz, Yaroslav Z. Khimyak, Karol P. Nartowski

PII: S0378-5173(23)00824-4
DOI: https://doi.org/10.1016/j.ijpharm.2023.123403
Reference: IJP 123403

To appear in: *International Journal of Pharmaceutics*

Received Date: 26 May 2023
Revised Date: 8 September 2023
Accepted Date: 9 September 2023

Please cite this article as: M. Nowak, A.J. Dyba, A.M. Gołkowska, A. Nieckarz, K. Krajewska, K. Malec, D. Iuga, B. Karolewicz, Y.Z. Khimyak, K.P. Nartowski, Probing fluconazole deposition inside mesoporous silica using solid-state NMR spectroscopy: crystallization of a confined metastable form and phase transformations under storage conditions, *International Journal of Pharmaceutics* (2023), doi: https://doi.org/10.1016/j.ijpharm.2023.123403

Title: Probing fluconazole deposition inside mesoporous silica using solid-state NMR spectroscopy: crystallization of a confined metastable form and phase transformations under storage conditions.

Maciej Nowak[1, *], Aleksandra J. Dyba[1, 2], Anna M. Gołkowska[1], Aleksandra Nieckarz[1], Karolina Krajewska[1], Katarzyna Malec[1], Dinu Iuga[4], Bożena Karolewicz[1], Yaroslav Z. Khimyak[3, *], †Karol P. Nartowski[1, 3]

1. Department of Drug Form Technology, Wroclaw Medical University, Borowska 211A, 50-556 Wroclaw, Poland

2. Institute of Pharmacy, University of Innsbruck, Innrain 52c, 6020 Innsbruck, Austria

3. School of Pharmacy, University of East Anglia, Norwich Research Park, NR4 7TJ Norwich, United Kingdom

4. Department of Physics, University of Warwick, CV4 7AL Coventry, United Kingdom

† Deceased Author

* Corresponding author

Abstract:

Encapsulation of molecules into mesoporous silica carriers continues to attract considerable interest in the area of drug delivery and crystal engineering. Here, MCM-41, SBA-15 and MCF silica matrices were used to encapsulate fluconazole (FLU), a pharmaceutically relevant molecule with known conformational flexibility, using the melting method. The composites have been characterized using ^{1}H, ^{13}C and ^{19}F NMR spectroscopy, nitrogen adsorption, PXRD and thermal analysis (DSC, TGA). Drug loading up to 50 wt.% allowed us to probe the crystallization process and detecting different local environments of confined FLU molecules. ^{19}F NMR spectroscopy enabled us to detect the gradual pore filling of silica with FLU and differentiate the amorphous domains and surface species. The use of the complementary structural and thermal techniques enabled to monitor crystallization of the metastable FLU form II in MCF. Using ^{1}H and ^{19}F NMR spectroscopy we observed pore-size dependent reversible dehydration/hydration behaviour in the MCM and SBA composites. As water content has considerable importance in understanding of physicochemical stability and shelf-life of pharmaceutical formulations, experimental evidence of the effect of API-water-carrier interactions on the API adsorption mechanism on silica surface is highlighted.

1. Introduction:

Confined crystallization using mesoporous silicas is recognized as an effective crystal engineering tool for controlling polymorphism and understanding of nucleation processes (Beiner *et al*., 2007; Ha *et al*., 2004; Nartowski *et al*., 2018, 2015; Zhang *et al*., 2020). During nucleation molecular clusters aggregate into more stable structures upon attaining the critical nuclei size comparable to mesopores diameters – both on a nanometer scale. Therefore, adjustment of pore diameter of mesoporous materials can be used to control the crystallization outcome, as the critical nuclei sizes can vary between polymorphs. Furthermore, the large surface area of the encapsulating host may affect the outcome through heterogenous nucleation at the pore walls (Ha *et al*., 2004). Several investigations regarding polymorph selectivity for model drugs have been carried out with the aid of nanoscale confinement using materials such as silicas or controlled pore glass (CPG). The work of Cheng *et al.* confirms the dependence of glass transition, cold-crystallization and melting of nifedipine on the confinement size. Depression of the glass transition temperature was observed for the CPG-confined nifedipine and a new polymorph was found in the 50-198 nm size pores (Cheng and McKenna, 2019). Moreover, the polymorphic transformation pathways have been found pore-size dependent and different from the “in bulk” conversion into form III, as described by Zhang *et al*. for polymorph-rich flufenamic acid (proceeding from the highly unstable form VIII which was stabilized by the nanoconfinement) (Zhang *et al*., 2020). Our previous works described control and stabilization of metastable forms of two highly flexible molecules – form V of indomethacin using

MCF (mesostructured cellular foams) and CPG (Nartowski *et al*., 2015), and form V of tolbutamide in MCM-41 (Nartowski *et al*., 2018). Ha *et al.* using anthranilic acid and 5-methyl-2-[(2-nitrophenyl)amino]-3-thiophenecarbonitrile (ROY) investigated the effect of critical nucleus size constraints on crystal nucleation. According to this study, the stabilization of metastable forms in the glass and polymer matrices was possible due to the large critical nuclei size of the stable forms (Ha *et al*., 2004). However, Beiner *et al.* applied nanoconfinement to stabilize not only a transient form III of acetaminophen, but also the most stable polymorph I. The authors attributed this phenomenon to the crystallization conditions, also pointing out a possible kinetic origin of the stabilization of the metastable form and interfacial effects on the crystallization kinetics (Beiner *et al*., 2007). Among the crystallization conditions affecting the end nanoconfined product Cao *et al.* named solvent properties, as they proposed conducting the process under solvent vapour. The crystallization of the metastable form of vortioxetine hydrobromide – form α – was preferred when using solvent vapours with large molecular volume such as methyl acetate, s-butanol, or n-propanol; possibly due to a significant spatial confinement effect (Cao *et al*., 2022).

A comprehensive understanding of confined crystallization processes requires the application of complementary characterisation methods such as powder X-ray diffraction (PXRD) and differential scanning calorimetry (DSC) to analyse the structure and thermal properties of the encapsulated nanocrystals. The incorporated species exhibit lack of or decreased long-range ordering as compared with bulk, noticeable as peak broadening and lower intensity of the reflections in diffractograms or melting point decrease (Ha *et al*., 2009). Solid-state NMR spectroscopy, highly sensitive to changes in local environment, aids in phase identification and analysis of molecular behaviour of the guest molecules and the guest-guest/guest-host interactions. Trzeciak *et al.* used various solid-state NMR methods to distinguish between mobile and rigid species of model pharmaceuticals (ibuprofen, flurbiprofen, and ketoprofen) loaded into MCM-41 via diffusion supported loading (DiSupLo) method (Trzeciak *et al*., 2020). Skorupska *et al*. investigated formation of confined cocrystals in the thermal solvent-free loading method as well using complex NMR analysis to investigate the behaviour of naproxen/picolinamide cocrystal as it has been found to separate when loaded into MCM-41 materials and embedded into SBA-15 (Skorupska *et al*., 2016). Nanoconfinement of praziquantel (PZQ) and its cocrystal with glutaric acid using a combination of NMR and other complimentary techniques was documented for SBA-15 where PZQ was found to be amorphous and the PZQ/glutaric acid cocrystal was found in a crystalline form. These findings have been associated with larger crystal lattice of PZQ over its cocrystal and stronger PZQ/GLU intermolecular interactions (Salas-Zúñiga *et al*., 2022). ^{1}H-^{13}C and ^{1}H-^{29}Si HETCOR experiments carried out by Azaïs *et al*. enabled monitoring of the encapsulated ibuprofen molecules mobility and characterization of the interaction between the loaded drug and the silica matrix (Azaïs *et al*., 2006). Careful design of the NMR experimental protocols, as shown by Azaïs *et al*., is crucial in order to efficiently characterize properties of investigated mesoporous materials, such as the proximity between the encapsulated drugs (ibuprofen, benzoic acid, and lauric acid) and the pore surface (Azaïs *et al*., 2009).

In this work we used fluconazole (FLU) as a model drug for the examination of nanoconfined phase behaviour. As a highly flexible molecule with significant conformational freedom, FLU is known as a prolific polymorph and solvate former (Nowak *et al*., 2022). Furthermore, FLU is a representative of fluorinated compounds which continue to attract considerable attention due to the modification of their lipophilicity, membrane permeability and, in consequence, bioavailability (Yerien *et al*., 2016). The presence of fluorine atoms facilitates a complex NMR analysis to further probe the local environment of the confined molecules. As shown in our previous work, ^{19}F solid-state NMR spectroscopy allows for monitoring confined crystallization within nanopores using flufenamic acid (Nartowski *et al*., 2016). Using ^{19}F NMR and ^{1}H-^{19}F HOESY MAS measurements, Skorupska *et al*. demonstrated the structure and molecular dynamics of a benzoic acid cocrystal with fluorinated benzoic acid encapsulated in MCM-41 and SBA-15 (Skorupska *et al*., 2015).

In this work we stabilised FLU in amorphous state for over 5 years using MCM-41 and SBA-15 while controlled formation and 5 years shelf stability was achieved for metastable FLU form II confined in MCF materials. Two different temperatures in ^{1}H-^{13}C CP/MAS experiments were used to probe changes in local mobility of confined species that undergo vitrification below 273 K. Using ^{19}F NMR spectroscopy we were able to identify FLU in three different molecular environments: crystalline, amorphous, and surface species, which corroborates our previous findings on flufenamic acid (Nartowski *et al*., 2016). As 14 out of 50 molecules approved by the Food and Drug Administration in 2021 for clinical use contained halogenated moieties, the investigation of the drug/host interactions using ^{19}F solid state NMR spectroscopy provides valuable insight into control over the complex processes that govern crystallization in nanoconfinement (Benedetto Tiz *et al*., 2022).

The interactions of water with pharmaceutical formulations and the effect of moisture/water content on the properties of pharmaceuticals have been investigated widely (Veronica *et al*., 2022). Exposure to moisture greatly affects the stability of drugs through hydrolysis or other water-mediated reactions even in solid dosage forms (Badawy *et al*., 2016; Hasegawa *et al*., 1975; Paszun and Stanisz, 2013). Moisture has also been documented to induce polymorphic transformation or hydrate formation in APIs, which in turn may result in changes in biopharmaceutical properties (Ando *et al*., 1992; Kato *et al*., 2006; Krueger *et al*., 2014; Otsuka *et al*., 1999; Paisana *et al*., 2016). The interest for investigating the effect of water on formulation components also stems from the documented enhanced molecular mobility, increased nucleation probability and subsequent crystallization/phase separation of APIs and polymers as a result of water uptake regarding *e.g*. solid dispersions (Konno and Taylor, 2008; Mehta *et al*., 2016; Ohtake and Shalaev, 2013). The presence of water might also influence the adsorption and migration of the drug in mesoporous silica carriers as well as their release profile as investigated by Mellaerts *et al.* using itraconazole and Nile red encapsulated into SBA-15 materials with co-adsorbed water (Mellaerts *et al*., 2011).

The aim of this work was to gain a molecular level understanding of fluconazole deposition and its crystallization in MCM-41, SBA-15 and MCF silica matrices. These findings are of pharmaceutical importance, as drug distribution inside nanocarriers and crystallization outcome can affect key parameters of drug formulation such as release profile, bioavailability or stability. In addition, the combined application of ^{1}H and ^{19}F MAS NMR spectroscopy enabled us to identify for the first time the reversible effect of hydration and dehydration on the distribution of confined phases (amorphous and surface species).

2. Materials and methods

2.1 Materials

Fluconazole (FLU) was a kind gift from pharmaceutical company PPF Hasco-Lek S.A. (Wroclaw, Poland). Pluronic P-123, n-hexadecyltrimethylammonium bromide (CTAB), 1,3,5-trimethylbenzene, tetraethoxysilane (TEOS), ammonia (37% wt.), sodium chloride, concentrated hydrochloric acid, methanol and ethanol were purchased from Sigma-Aldrich and were used without further purification.

2.2. Mesoporous materials synthesis:

MCF particles were synthesised using method elaborated by Han *et al*. (Han *et al*., 2007). 8 g of Pluronic P-123 was dissolved in 150 mL of 1.5 M HCl solution in a polypropylene bottle at room temperature. 8 g of 1,3,5-trimethylbenzene was added to the solution and then the bottle was placed in a water bath which was heated to 40 °C, constant stirring was applied for two hours. Then, 18.4 mL of TEOS was added dropwise and the contents were stirred for 5 minutes. The obtained solution was aged at 40 °C for 20 minutes without stirring, followed by the addition of 92 mg of NH_4F and then further aging at 100 °C for 24 hours. The obtained product was filtered and then rinsed with water and ethanol (EtOH). The material was dried in the oven at 40 °C for 24 hours. The last stage of the synthesis was calcination at 900 °C for 10 hours in air atmosphere.

SBA-15 porous host was synthesised using procedure published by Zhao *et al.* (Zhao *et al*., 1998) with the addition of NaCl in order to obtain a material with higher hydrothermal stability as described by Li *et al.* and Ryoo *et al*. (Li *et al*., 2007; Ryoo and Jun, 1997). 4 g of Pluronic P-123 and 11 g of NaCl were dissolved in 125 mL of 2 M HCl solution in a polypropylene bottle at room temperature. Then, 8.46 mL of TEOS was added and the contents were stirred at 40 °C for 20 hours. The solution was placed in an oven at 90 °C for 24 hours. The product was filtered, rinsed with water, and then left to dry. The calcination process was carried out at 500 °C for 8 hours in air.

MCM-41 particles were synthesised using method reported by Grün *et al.* (Grün *et al*., 1999). 5 g of CTAB was dissolved in 28.7 mL of water. A mixture of 120 g of EtOH and 97.7 g of 10 % ammonia was added to the CTAB solution. The obtained solution was stirred for 15 minutes. Then, 9.4 g of TEOS was added followed by 24 hours of stirring at 40 °C. The formed precipitate was filtered, rinsed with methanol and water, and dried in an oven at 90 °C overnight. The calcination process was carried out at 500 °C for 5 hours in air atmosphere.

2.3. Loading fluconazole into the mesoporous materials: The loading process was carried out using a sand bath equipped with an external temperature sensor. Each sample was transferred into a crucible and then placed in

the sand heated up to 150 °C, *ca.* 10 °C above the melting point of fluconazole (141 °C). The drug/material mixture was kept in the described conditions for 10 minutes with constant stirring using a spatula. This procedure was applied to prepare all mixtures of MCF, SBA and MCM with fluconazole in different material to drug ratios: 50-50, 60-40, 70-30, 75-25, 80-20 and 85-15 (wt.%).

2.4. Powder X-ray diffraction: Powder X-ray diffraction patterns were recorded employing a D2 Phaser diffractometer (Bruker) with Cu Kα radiation (1.5418 Å) and a LynxEye detector. Each composite was weighed in an amount corresponding to approx. 25 mg of the neat silica material enabling for quasi quantitative assessment of the silica reflections assessed in the low angle setup. To characterize the structure of the incorporated fluconazole all samples were measured in the range of 2θ 5-36° with 0.02° increment and 2 s irradiation time per step. Low angle diffraction patterns for the MCM and SBA materials (loaded and not-loaded) were recorded in the range of 2θ 0.65-8° with 0.02° increment and 1 s irradiation time per step.

2.5. Differential scanning calorimetry: A DSC 214 Polyma calorimeter (Netzsch) was used to record the DSC thermograms. 5-6 mg of the samples were weighed and then placed in standard 100 µl aluminium pans with pierced lids and an empty pan with a pierced lid used as the reference. The heating range for all the samples was 0-150 °C with a heating rate of 5 K/min and the nitrogen flow of 50 mL/min.

2.6. Thermogravimetric analysis: TGA measurements were performed using TG 209 F1 Libra Thermobalance (Netzsch). The sample weight of the loaded materials was 8-9 mg. The materials were placed in aluminium oxide crucibles and heated from 25 to 800 °C. The heating rate was 10 K/min for up to 300 °C, then 20 K/min for up to 800 °C. Upon reaching 800 °C, the temperature was kept constant for 5 additional minutes of the measurement. Nitrogen flow applied during the measurements was 50 mL/min; for the isothermal conditions an additional air flow of 25 mL/min was added.

2.7. Gas sorption analysis: Adsorption-desorption isotherms of nitrogen were obtained using a Nova 2200e Surface Area and Pore Size Analyzer (Quantachrome, Hook) at -196 °C. All samples were outgassed prior to the analysis under a high vacuum at 40 °C for 12 hours. The pore size distribution analysis was performed using the Barrett–Joyner–Halenda (BJH) algorithm using the Broekhoff-de Boer method for the estimation of adsorbed statistical film thickness. The BET specific surface area was calculated using molecular area of nitrogen of 0.162 nm^2 over a relative pressure range from p/p_0=0.05 to 0.20 assuming a monolayer coverage of the material surface. For all three hosts, the size of the pores was calculated from the adsorption branch of the isotherms. The size of the interconnecting pores windows of the MCF host was calculated from the desorption branch of the isotherm (Han *et al*., 2007; Lukens, *et al*., 1999).

2.8. Solid-state NMR: Solid-state NMR experiments were acquired using a Bruker AVANCE III solid-state NMR spectrometer equipped with a triple resonance probe operating at 400.23 MHz for ^{1}H, 376.57 MHz for ^{19}F and 100.64 MHz for ^{13}C (9.4 T). Materials were packed to 4 mm zirconia rotors and spun at 10 kHz MAS rate. All host-guest composites were analysed with single pulse ^{1}H, ^{19}F and ^{1}H-^{13}C cross-polarization/magic angle spinning (CP/MAS) solid-state NMR experiments (^{1}H π/2 pulse length 3.5 µs, ^{19}F π/2 pulse length 3.6 µs). ^{1}H-^{13}C CP/MAS spectra were acquired using RAMP CP pulse sequence with contact time of 2 ms and SPINAL64 decoupling during acquisition. The Hartmann-Hahn conditions were set with hexamethylbenzene (HMB). The ^{13}C chemical shifts were recorded with respect to TMS and ^{19}F chemical shifts were recorded with respect to $CFCl_3$ setting PTFE peak to -122 ppm. During measurements 16 increments were acquired with a maximum time delay of 20 s. Spectra were recorded at 25 °C and -40 °C. The data were fitted using Bruker Topspin 3.1 software. Further ^{1}H and ^{19}F analysis of FLU loaded composites was performed using a Bruker NEO spectrometer equipped with 1.3 mm triple resonance probe operating at 850.22 MHz for ^{1}H and 799.94 MHz for ^{19}F (20 T) at the UK National high-field solid-state NMR facility at Warwick. Materials were packed to 1.3 mm zirconia rotors and spun at an MAS rate of 60 kHz. All composites were analysed using single pulse ^{1}H and ^{19}F experiments. 16 scans were acquired using a recycle delay of 20 s at 25 °C.

2.9. Theoretical monolayer loading capacity (MLC): The theoretical MLC for FLU-silica composites was calculated using the equation proposed by Azaïs *et al.* (Azaïs *et al*., 2006):

$$X_m = \frac{SSA\ x\ 10^{20}\ x\ MW}{S_c\ x\ N_a}$$

where *SSA* is the specific surface area of silica particles (m^2 g^{-1}), *MW* is the molecular weight of adsorbate (g mol^{-1}), S_c is the contact surface area of individual adsorbate molecule ($Å^2$) and N_A is Avogadro constant. The dimensions of FLU molecules were calculated using the Olex2 v1.5 software (Dolomanov *et al*., 2009) and the largest wall surface of the molecular bounding box was adopted as the S_c.

3. Results and discussion

3.1. Loading efficiency of silica hosts

The starting form of FLU used for loading was identified as the polymorphic form I. This is the most stable form of FLU with melting point at *ca*. 141 °C. The drug was loaded into MCM-41, SBA-15, and MCF silicas with the pore diameter of *ca.* 3.2, 7.5 or 24 nm, respectively, using the melting method. Changes in pore diameter and total pore volume according to the drug load were determined using nitrogen adsorption-desorption analysis. A decrease in pore diameter and total pore volume followed the increase of drug load for all materials (ESI Fig. S1, Table 1). Low-angle PXRD patterns measured for the loaded materials show a gradual attenuation of the d[100] reflections for MCM and SBA (ESI Fig. S2A and S3A) confirming drug encapsulation into the materials pores.

Table 1. Drug content in the MCM-41, SBA-15 and MCF hosts and structural parameters of the host after loading.

	FLU (g/g)	V_{total} [cm^3/g]	d_{pore} [nm]	S_{BET} [m^2/g]
MCM-41	N/A	0.697	3.18	983.8
MCM-FLU 85-15	0.129	0.406	3.06	689.3
MCM-FLU 80-20	0.193	0.320	2.82	566.7
MCM-FLU 75-25	0.226	0.218	2.58	384.3
MCM-FLU 70-30	0.280	0.138	2.58	148.6
MCM-FLU 60-40	0.370	0.066	1.22	36.4
MCM-FLU 50-50	0.433	0.055	N/A	22.1
SBA-15	N/A	1.118	7.50	514.1
SBA-FLU 85-15	0.126	0.589	6.38	327.4
SBA-FLU 80-20	0.170	0.414	5.87	267.3
SBA-FLU 75-25	0.212	0.348	5.56	231.2

SBA-FLU 70-30	0.255	0.299	5.21	195.7
SBA-FLU 60-40	0.363	0.155	4.91	86.8
SBA-FLU 50-50	0.449	0.064	4.91	15.9
MCF	N/A	1.867	24.04	337.7
MCF-FLU 85-15	0.133	1.083	24.06	236.0
MCF-FLU 80-20	0.190	0.990	24.21	229.6
MCF-FLU 75-25	0.233	0.884	24.09	190.8
MCF-FLU 70-30	0.254	0.842	23.83	190.9
MCF-FLU 60-40	0.406	0.716	24.24	169.3
MCF-FLU 50-50	0.489	0.362	24.21	73.06

3.2. Stabilisation of amorphous FLU in MCM-41 and SBA-15

Thermal behaviour of FLU in bulk state was investigated previously by Desai and Dharwadkar as well as by our group for amorphous solid dispersions. Amorphous FLU crystallizes just after one hour into FLU form II or the FLU hydrate depending on the humidity (Desai *et al*., 2002; Nowak *et al*., 2019). Mesoporous MCM-41 and SBA-15 carriers inhibited the crystallization of FLU leading to the stabilization of the amorphous phase for at least 5 years regardless of the drug content within the pores. Combined results from the PXRD measurements and DSC analysis indicated the confinement of the drug molecules in the mesoporous carrier (leading either to a stable amorphous phase or to confined crystals) or crystallization outside the pores. Careful evaluation of thermograms should be carried out as a melting point depression can be observed for pore-confined molecules according to the Gibbs-Thomson equation (Ha *et al*., 2009; Hamilton *et al*., 2012; Knight *et al*., 2019). The melting point of the drug outside the pores has a similar value to that of the bulk crystals. Amorphization or decrease of long-range ordering due to formation of nano-sized crystals can be observed for the confined molecules as broadening of the PXRD reflexes (Ha *et al*., 2004). For the MCM-FLU composites with material-drug ratio up to 70-30 PXRD patterns show a "halo" characteristic for amorphous solids. MCM-FLU 60-40 exhibits low intensity reflections and the MCM-FLU 50-50 pattern shows peaks at 7.8, 15.6 and 16.2 2θ, which could be assigned to FLU polymorph II. (ESI Fig. S2B) However, the DSC thermogram (ESI Fig. S2C) for the MCM-FLU 60-40 does not show any thermal events related to the melting of FLU. An endothermic event starting at 132.5 °C for MCM-FLU 50-50, which is close to the temperature of the bulk melting (135.6 °C), confirms the crystallization of FLU outside the pores. PXRD patterns (ESI Fig. S3B) recorded for SBA-FLU show FLU amorphization for samples up to 60-40 ratio and crystallization of the drug outside the pores for the SBA-FLU 50-50. This is corroborated by a small endothermic event at *ca*. 136 °C that might be assigned to the melting of FLU deposited on the outer surface of the particles. No thermal events related to FLU melting occurred for the rest of the materials (ESI Fig. S3C). TGA measurements (ESI Fig. S2D and S3D) follow the gradual increase of the drug content. Calculated first derivatives

(DTG) (ESI Fig. S4) for the MCM-FLU 50-50 and 60-40 and the SBA-FLU 50-50 showed the FLU decomposition onset at *ca*. 150 °C, *i.e.* a temperature similar to the thermal degradation of a neat FLU, indicating that part of the drug is not confined within the pores. The decomposition of FLU confined within MCM-41 and SBA-15 materials loaded with lower drug content started at a higher temperature (at *ca.* 190 or 175 °C respectively) which confirms FLU encapsulation.

^{1}H-^{13}C CP/MAS NMR spectra of FLU polymorphs supported by CASTEP calculations were described in detail in our previous work (Nowak *et al*., 2022). Based on previously calculated isotropic chemical shifts for FLU polymorphs in bulk state, four spectral regions can be depicted (Fig. 1 and ESI Fig S6). First region at 50-80 ppm was assigned to the propylene backbone (C7, C8, C9). Two regions were assigned to the difluorobenzene ring at 100-135 ppm (C2, C3, C4, C6) and at 155-165 ppm for the carbons bound to fluorine atoms (C1, C5). The fourth region at 140-145 ppm was assigned to the carbons located in the triazole rings (C10, C11, C12, C13). The NMR spectra of MCM-FLU and SBA-FLU composites were recorded at 25 and -40 °C. The decrease of the acquisition temperature to -40 °C resulted in an increased signal-to-noise ratio across all investigated materials and drug loadings (compare Fig. 1 and ESI Fig S6). These data indicated that at RT the FLU molecules are in highly dynamic state reducing the efficiency of polarization transfer during ^{1}H-^{13}C CP/MAS experiments. In contrast, once the confined FLU molecules have undergone vitrification, it allowed us to identify their dynamic state. Based on the observed widening of ^{13}C resonances, total drug amorphization took place in all MCM-41 and SBA-15 materials except for the MCM-FLU 50-50, where peaks characteristic for FLU form II loaded outside the pores of the hosts were detected, in agreement with the PXRD results.

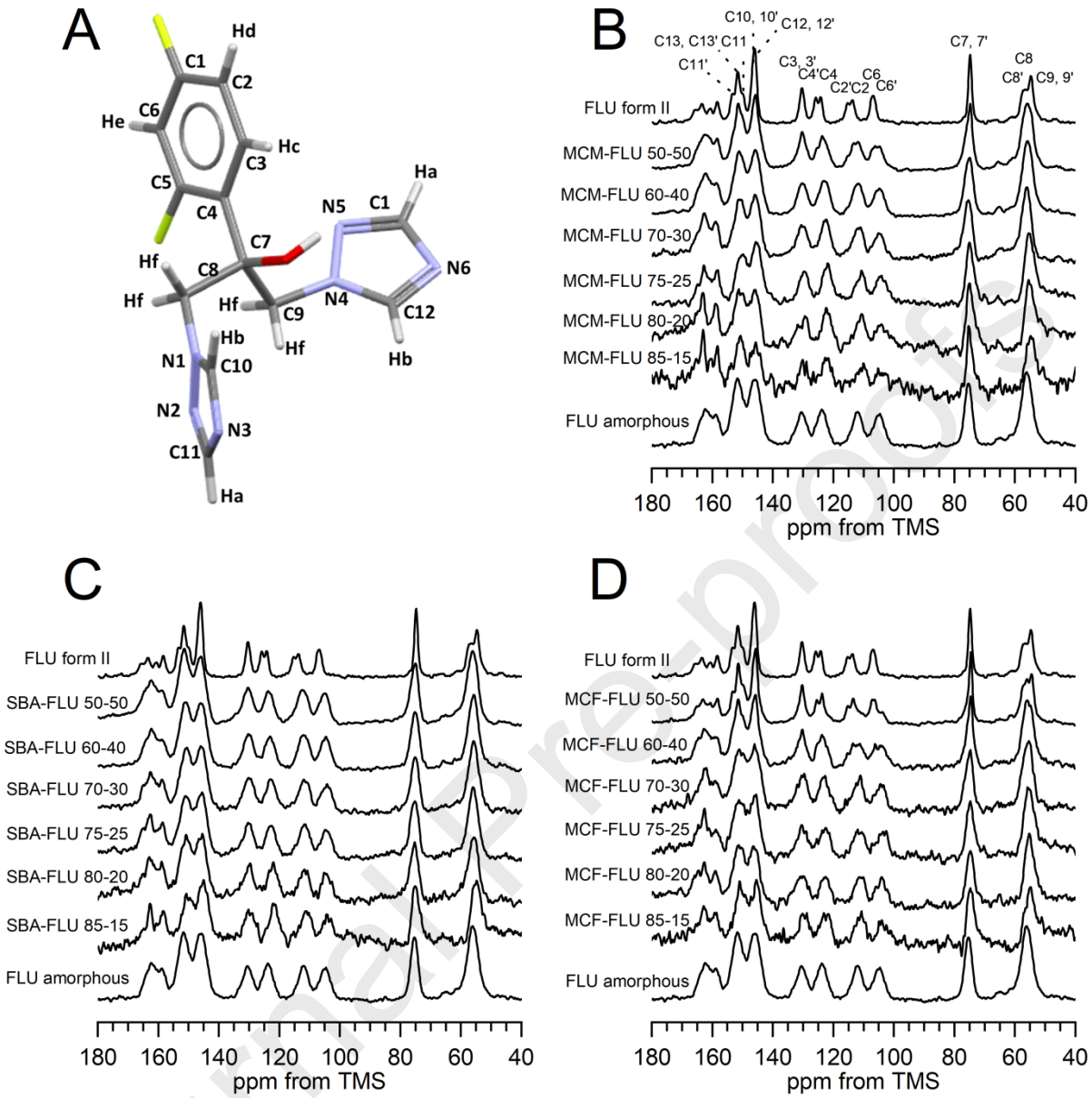

Figure 1. Molecular structure of fluconazole with carbon and nitrogen atom labelling (A); ^{1}H–^{13}C CP/MAS NMR (9.4 T) spectra with different host/drug ratios recorded at -40 °C for MCM-41 (B), SBA-15 (C) and MCF (D).

3.3. Crystallization of FLU in MCF

Nitrogen adsorption-desorption measurements show a decrease in total pore volume with an increasing drug content (Table 1). Depending on the drug content PXRD diffractograms exhibit the drug either in its amorphous state (up to MCF-FLU 70-30) or in the crystalline form (ESI Fig. S5A). The beginning of FLU crystallization can be observed for MCF 60-40 as low intensity reflexes are emerging from the baseline. The PXRD pattern of MCF-FLU 50-50 shows an increased content of the crystalline form and broadening of the reflexes indicates the appearance of submicron crystals. DSC measurements (ESI Fig. S5B) also point to drug crystallization in the MCF-FLU 60-40 and 50-50 materials which is observed as endothermic events at 115.8 and 119.2 °C, respectively. This is expected for confined nanocrystals (Jiang and Ward, 2014). Lack of any thermal event at temperature above 130 °C confirms the total drug encapsulation. As confirmed by TGA and DTG results (ESI Fig. S5C and ESI Fig. S4), drug degradation onset temperature for the MCF-FLU materials was shifted towards higher temperatures as compared to the degradation temperature of neat FLU. Despite the smallest pore area among the investigated materials, only MCF was able to fully load FLU inside the pores. This is in agreement with

previous reports where, despite an increase in surface area, loading efficiency decreased with decreasing pore diameter. This is due to the spatial constraint imposed by small diameter of pores (Andersson *et al*., 2004; Bavnhøj *et al*., 2019; Horcajada *et al*., 2004).

The NMR spectra for the MCF-FLU materials were recorded at -40 and 25 °C (Fig. 1 and ESI Fig. S6). The spectra are in agreement with the PXRD and thermal measurements. MCF-FLU materials up to the 70-30 silica/FLU ratio contained amorphous FLU (as expressed by the peak broadening), while MCF-FLU 60-40 and 50-50 exhibit peaks closely resembling FLU form II with evident peak splitting in MCF-FLU 50-50 due to crystallization of FLU form II with two conformationally distinct molecules in the asymmetric unit (Z'=2). It is important to note that this polymorph is a metastable form of FLU (Nowak *et al*., 2022).

3.4. Probing of FLU crystallization using ^{19}F NMR spectroscopy

Our previous work allowed us to obtain detailed insight into the mechanism of confined crystallization of flufenamic acid using a combination of ^{19}F NMR spectroscopy and nitrogen adsorption analysis as the drug was found in three dynamically different environment as highly mobile surface species, confined amorphous state or confined crystals (Nartowski *et al*., 2016). Here, this approach was used to monitor the crystallization process of FLU. The ^{19}F NMR spectra (20 T) (ESI Fig. S7) of bulk FLU form I (Z'=1) and II (Z'=2) show a considerable difference between these forms. Although FLU contains two fluorine atoms attached on benzene ring, only one peak can be observed at -122.8 ppm for FLU form I. The spectrum of form II with two molecules in asymmetric unit exhibits four distinct peaks at -118.7, -120.2, -121.6 and -123.4 ppm. FLU-loaded silica scaffolds of different porosity exhibited gradual increase of ^{19}F MAS NMR signal intensity with increasing content of FLU inside the pores (Fig. 2, ESI Fig. S9). In the MCM-41 and SBA-15 materials characterized as amorphous by PXRD, two peaks were observed in the ^{19}F MAS NMR spectra (-121.8 and -126.9 ppm) confirming the presence of FLU species in two distinct environments. The peak at -121.8 ppm can be assigned to the amorphous FLU as its chemical shift corresponds to that of neat amorphous FLU (ESI Fig. S7A). The intensity of this peak increases in line with the drug load and indicates that the drug deposition inside the pores occurs gradually, in agreement with the N_2 adsorption data. The intensity of the peak at -126.9 ppm is the highest for the respective drug/host ratios: MCM-FLU 75-25, SBA-FLU 70-30 and MCF-FLU 80-20 (ESI Fig. S8, S10-11). Similar behaviour was observed for flufenamic acid incorporated into mesoporous silica (Nartowski *et al*., 2016), where gradual saturation of silica surface phase was confirmed by ^{19}F NMR. In contrast, for MCF hosts characterized by a lower surface area compared with SBA-15 or MCM-41 silicas, only slight changes in the intensity of the peak at -126.9 ppm are observed for the FLU loaded materials up to 30 wt.% drug content. As silicas pore surface area decreases with increasing pore diameter, the decrease in surface phase contribution is expected, especially for the MCF host. The determined intensities of the individual deconvoluted ^{19}F peaks attributed to the crystalline phase, in pore amorphous phase and disordered surface phase were summed and the population of each phase was calculated. The amount of FLU allowed to fill the surface, referred to as the monolayer loading capacity (MLC) (Azaïs *et al*., 2006; Dening and Taylor, 2018), has been calculated. Experimental MLC was calculated as follows: (i) for a given system (e.g. SBA-FLU), the sample with the largest FLU population assigned to the surface phase was selected based on the deconvoluted ^{19}F MAS NMR spectra (e.g. SBA-FLU 70-30); (ii) the mass of fluconazole corresponding to the surface phase was calculated from the percentage of surface phase population (e.g. 37 %) relative to the total amount of FLU loaded in the selected sample (e.g. 0.255 g); (iii) the ratio of the mass of fluconazole corresponding to the surface phase (e.g. 0.094 g) to the mass of pure silica in the given sample (e.g. 0.745 g) was calculated. The experimental MLCs were determined to be 0.149, 0.126 and 0.091 (g/g) for MCM-41, SBA-15, and MCF respectively, which is in line with the expected decrease in surface phase contribution. According to the ^{19}F NMR spectra, simultaneous growth of both the amorphous and surface phase, even for low drug loads, with gradual saturation of the surface is evident in the studied systems (especially in MCM and SBA). We observed this behaviour in other materials e.g. flufenamic acid loaded in porous silicas, where both amorphous and surface phases were located in the pore space (Nartowski *et al*., 2016). In addition, the theoretical MLC was calculated (ESI Fig. S12, ESI Table S1) for MCM-41 (0.405-0.448 g/g), SBA-15 (0.212-0.234 g/g), and MCF (0.139-0.154 g/g). Experimental MLC values were found to be lower than theoretical MLCs. However, the proposed model for theoretical MLC calculation is somewhat simplified and assumes that the entire surface is available for the adsorbate. This may not be accurate for mesoporous materials, as theoretical MLC calculations utilise nitrogen adsorption data (it is important to note that FLU molecules are larger than N_2). These calculations also do not take into account the true density of the molecules being incorporated or the loading method used (Bavnhøj *et al*., 2019; Vraníková *et al*., 2020).

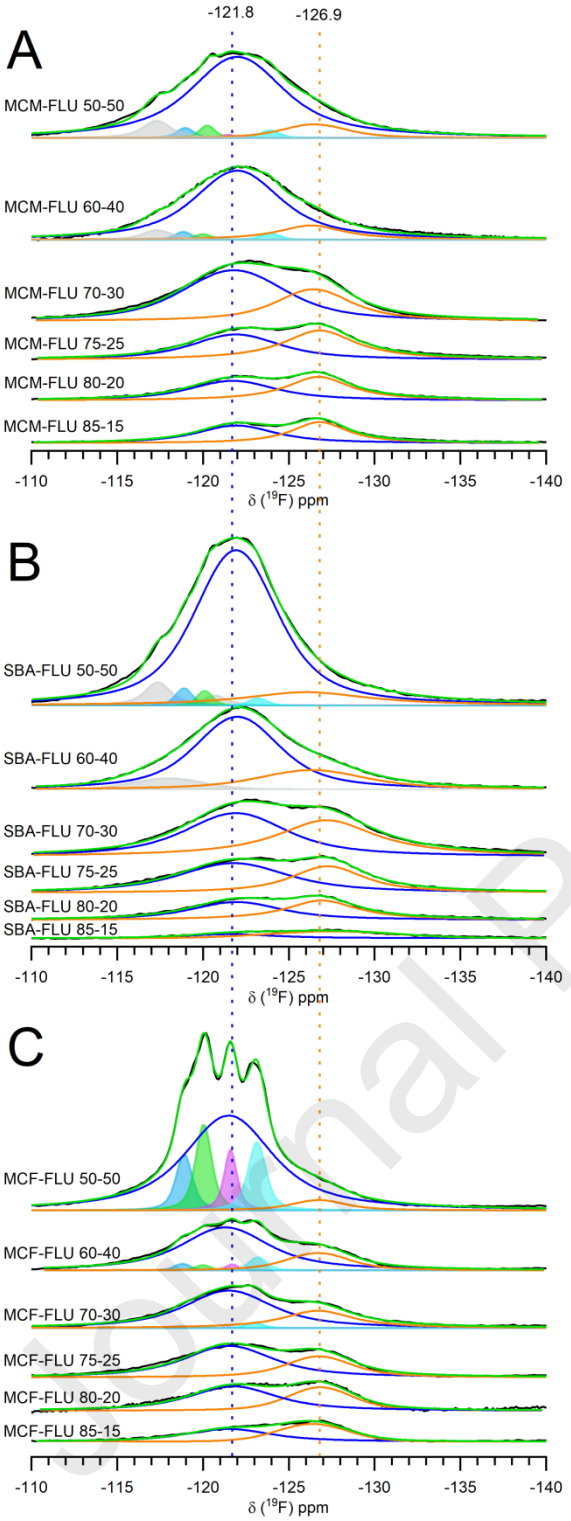

Figure 2. Deconvoluted ^{19}F MAS NMR (20 T) spectra of FLU-loaded MCM (A), SBA (B) and MCF (C) materials with different drug loads. Black lines – experimental; green lines – cumulative; blue - amorphous; orange – surface. Filled AUC – crystalline: blue, green, magenta and cyan – FLU form II; grey – additional crystalline phase.

Along with PXRD and DSC measurements, ^{19}F NMR spectroscopy allows for observation of the FLU crystallization process. Crystalline FLU form II has two molecules in the asymmetric unit (Z'=2) and its four fluorine atoms do not exhibit magnetic equivalence, hence we observe four distinct peaks in the ^{19}F NMR spectrum. Emerging peaks corresponding to FLU form II (ESI Fig. S7B) can be observed in the MCM-FLU 50-50

and SBA-FLU 50-50 spectra at -119.0, -120.2, -121.5 and -123.9 ppm. An additional peak is observed at -117.0 ppm corresponding to the FLU hydrate (ESI Fig. S7A). First signs of crystallization can also be detected at the 40 wt.% drug loading by a minor peak arm elevation in the -116 to -122 ppm region in comparison to the MCM-FLU and SBA-FLU 70-30 spectrum. For the MCF FLU-loaded materials, the ^{19}F MAS NMR spectra exhibit crystallization signs starting with the emerging peak at -123.9 ppm for the MCF-FLU 70-30 material. The materials loaded with 40 and 50 wt.% of FLU show distinct peaks characteristic of FLU form II as corroborated by the PXRD data. *Ca*. 3-5% of crystalline FLU was found in MCM and SBA hosts while *ca.* 20% of FLU form II was found in MCF composites as quantified by ^{19}F peaks deconvolution. The increase of the crystalline component is followed by the decreased intensity of the peak corresponding to the FLU surface species. The content of the crystalline phase in the MCM-FLU 60-40 material is estimated at only 3.4%. Considering the possible close contact of the crystalline species with the non-crystalline phase that exhibits an increased mobility during heating, the crystalline phase might dissolve, rather than melt, over the course of the DSC measurement and would not exhibit a visible melting point.

^{19}F solid-state MAS NMR spectra were recorded using two different field strengths: 20 T (at 25 °C) and 9.4 T (at 25 and -40 °C). Figures S8, S10 and S11 display gradual changes of deconvoluted peak intensity assigned to surface, amorphous and crystalline domains with increasing FLU loadings. Calculation of relative populations of components with different levels of ordering enabled us to observe the temperature-dependent changes of phase contributions as indicated by the increase (*ca*. 10%) of amorphous phase content at -40 °C and simultaneous decrease of the surface species contribution in the MCF-FLU materials. For the MCM-FLU composites these changes are more pronounced, with a maximum difference up to 20% for MCM-FLU 70-30. For the SBA composites such evident changes were not observed (maximum difference of *ca*. 7% for SBA-FLU 70-30).

3.5. Understanding of phase transformations of confined pharmaceuticals upon storage

The ^{19}F NMR spectra also showed differences between fresh and stored samples of the loaded silicas (Fig. 3). The water content in the FLU materials with 25 wt.% drug loading was found to be 0.55, 0.41 or 0.10 wt.% for the MCM, SBA and MCF composites, respectively (ESI Fig. S13). The materials were dried under controlled conditions to investigate the effect of humidity on FLU organisation in the pores. The phase distribution of FLU species was found to depend on the hydration level of the materials.

Additionally, ^{1}H NMR spectra of the FLU composites were recorded. In accordance to Malec *et al.* we could distinguish specific regions in the ^{1}H solution-state NMR spectra that can be assigned to the FLU triazole rings (Hb, Ha), the difluorobenzene rings (Hc+e, Hd) and the propylene backbone (Hf) (Fig. 1A) (Malec *et al*., 2023). These designated regions are in agreement with isotropic chemical shifts for three polymorphic forms of FLU (form I, II and IV) calculated using CASTEP. These forms show different molecular conformations (ESI Fig. S14, ESI Table S2). For the MCM-FLU composites stored at 50-60% RH (the RH condition in the lab) the amorphous phase (78%) is more populated than surface species (22%) based on ^{19}F NMR spectra. After oven drying at 75 °C for 30 min (water removal) an inversion of the phase distribution was observed with the amorphous phase content of 49 % and the surface species content of 51 %, which may be explained by an increase in the surface area available for FLU molecules, as it is no longer occupied by water molecules. Afterward, the materials were exposed to atmospheric humidity and the phase contribution reversed again, reaching the contribution of phases at 66 and 34% for amorphous and surface phases, respectively. According to a previous study (Skorupska *et al*., 2014), the exposure of MCM with incorporated ibuprofen (IBU) to elevated humidity leads to penetration of the water molecules deep into the material pores and even partial expulsion of IBU from the pores. ^{1}H and ^{13}C CP/MAS NMR measurements performed in another study confirmed changes in the molecular mobility of IBU incorporated in MCM-41 depending on the presence of water, also noting the reversibility dependent on drying or exposure of the materials to atmospheric humidity (Gackowski *et al*., 2021). The possibility of water diffusion into the pores with the incorporated drug further supports the possibility of changes in the distribution of FLU phases in silica materials. Additionally, according to the differences observed in the ^{1}H–^{13}C CP/MAS NMR spectra recorded at different temperatures (Fig. 1, ESI Fig. S6), FLU molecules inside the pores are not in a static state, even at RT (Azaïs *et al*., 2006; Babonneau *et al*., 2004), which allows for the changes in a phase contribution. The increase in temperature during the drying of the materials further affects the mobility of the molecules by facilitating the redistribution of FLU species from the amorphous to the surface phase. Changes in the ^{1}H NMR

spectra of dried MCM composites were also observed as peak broadening which was found to be reversible upon material rehydration. Similar observations were made for the SBA-FLU materials as the relative populations of amorphous and surface species content, based on the ^{19}F NMR spectra, changed from initial values of 45% and 55%, respectively, to 29% and 71% upon drying of the samples. Rehydration of these materials resulted in the expected reversal of the phase contribution with the amorphous phase content of 37% and the surface species content of 63%. The ^{1}H NMR spectrum recorded for the dried SBA-FLU composites exhibits similar peak broadening as in the MCM composites. However, the spectrum recorded for the rehydrated SBA material shows only minor changes in peak width, indicating that a longer contact time with water may be required to fully redistribute the phases. For the MCF-FLU materials the contribution of the amorphous and surface species (initially 82 and 18%, respectively) based on the ^{1}H and ^{19}F NMR spectra did not exhibit significant differences upon oven drying at 75 °C for neither 30 nor 120 minutes. This is not unexpected, as water content in MCF-composites is much lower than that of MCM-41 and SBA-15, so competition between water and FLU for the available surface was not observed.

These hydration/dehydration dependent changes in phase distribution of encapsulated drug species might stem from the forces that govern the drug/host, drug/water and water/host interactions. According to Delle Piane *et al*., the exposed silanol functional groups located on the silica pore surface exhibit high affinity for water (Delle Piane *et al*., 2014b, 2014a). This is further supported by experimental studies using NMR spectroscopy, where various local environments of water incorporated in silica matrices are detected, including a phase with high affinity for the silica surface (Grünberg *et al*., 2004; Pajzderska *et al*., 2014). Therefore, a competition adsorption of water and drug species is likely to take place at the silica surface. Dehydration of the composites may increase the access to pore surface for FLU molecules. This, in turn, will allow for higher population of FLU surface species observed in the ^{19}F NMR spectra for oven dried MCM and SBA materials (Gackowski *et al*., 2021).

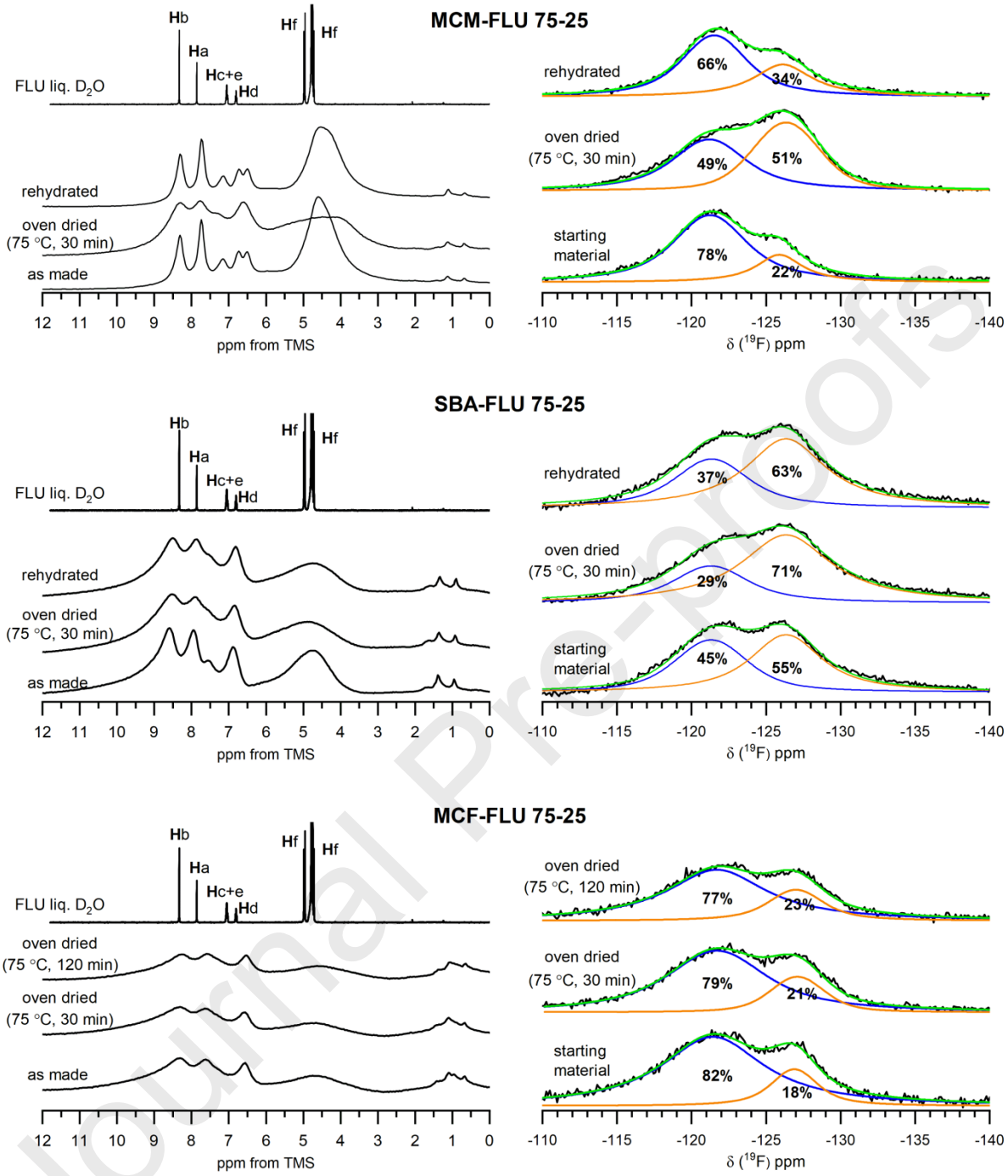

Figure 3. ^{1}H MAS NMR (20 T) spectra (left) and ^{19}F MAS NMR (20 T) spectra (right) of MCM, SBA and MCF FLU-loaded materials recorded during hydration/dehydration studies. Phase content of amorphous (blue) and surface (orange) species is marked as percentages of the AUC.

4. Conclusions

Mesoporous silica can be used as platforms for directed crystallization. In our work MCM-41, SBA-15 and MCF silica matrices were used to encapsulate fluconazole using the melting method. Using structural and thermal analysis we have confirmed that amorphous FLU can be stabilized by nanoconfinement in MCM and SBA silicas while crystallization of fluconazole form II was confirmed inside the MCF pores. The application of high-field ^{19}F solid state NMR spectroscopy for monitoring the local environment of nanoconfined FLU has been demonstrated in this work. Three different domains of FLU molecules have been identified and quantified:

surface, amorphous and crystalline (Scheme 1B-D). Pore size dependent specific changes in phase contribution were found for the MCM and SBA composites. As these materials are characterized by higher pore surface area than MCF, a gradual increase in contribution of the FLU amorphous and surface species is observed in line with the drug to silica ratio. The surface saturation for MCF matrices was found to occur at lower drug loadings due to MCF lower pore surface area compared with other composites used in this study. ^{19}F solid-state NMR spectroscopy allowed for detection of encapsulated crystalline FLU species inside the mesopores of MCF. At 30

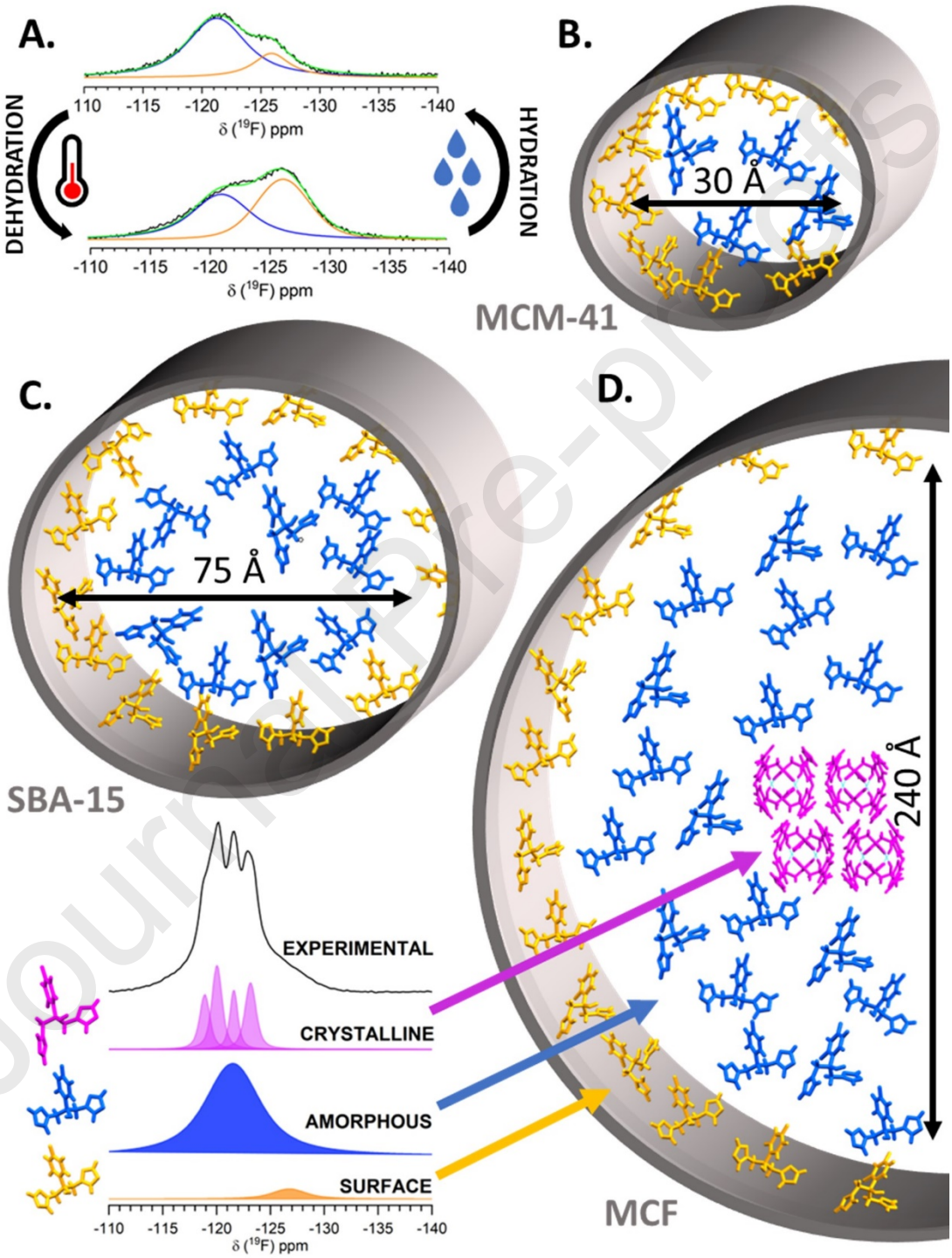

Scheme 1. The effect of hydration level on FLU phase distribution (^{19}F MAS NMR) in MCM-FLU 75-25 (A). Schematic representation of FLU phases inside mesoporous materials based on N_2 adsorption data and ^{19}F NMR analysis (B, C and D).

wt.% drug content first signs of FLU crystallization can be observed in the ^{19}F NMR spectrum, while for the 40 and 50 wt.% drug loads all four peaks assigned to FLU form II are identified.

To the best of our knowledge, the effect of pore size on the hydration/dehydration processes on phase behaviour of silica encapsulated FLU monitored by ^{19}F solid-state NMR is described here for the first time (Scheme 1A). For MCM-41 and SBA-15 based composites, reversible changes in the population of different FLU domains were observed due to the possible competition adsorption with water molecules. With the emerging role of halogenated new chemical entities as pharmaceutical agents (Benedetto Tiz *et al*., 2022), this work further highlights the application of ^{19}F solid-state NMR spectroscopy to monitor the nucleation of nanoconfined guest molecules and probe the complex interactions of drugs with pharmaceutically relevant carriers. The engineering of mesoporous silica hosts coupled with the experimental evidence of humidity influence on the different drug environments in nanoconfinement calls for further studies investigating the impact of storing conditions on the stability of novel pharmaceutical formulations based on this type of composites.

CRediT authorship contribution statement

Maciej Nowak: Conceptualization, Formal analysis, Investigation, Writing - Original Draft, Visualization, Funding acquisition. **Aleksandra J. Dyba:** Analysis, Investigation, Writing - Original Draft. **Anna M. Gołkowska:** Analysis, Investigation, Writing - Review & Editing. **Aleksandra Nieckarz:** Analysis, Investigation, Writing - Review & Editing. **Karolina Krajewska:** Analysis, Investigation, Writing - Review & Editing. **Katarzyna Malec:** Analysis, Investigation, Writing - Review & Editing. **Dinu Iuga:** Analysis, Investigation, Writing - Review & Editing. **Bożena Karolewicz:** Analysis, Investigation, Writing - Review & Editing. **Yaroslav Z. Khimyak:** Analysis, Conceptualization, Methodology, Investigation, Writing - Review & Editing, Funding acquisition. **Karol P. Nartowski:** Conceptualization, Methodology, Investigation, Writing - Review & Editing, Supervision, Funding acquisition.

Acknowledgements

The authors would like to thank the Laboratory of Elemental Analysis and Structural Research at the Faculty of Pharmacy at the Wroclaw Medical University for the access to PXRD, DSC, and TGA instruments. A.J.D. and A.M.G. thank the National Science Centre in Poland for a postgraduate scholarship via a MOZART grant (UMO-2020/01/Y/ST4/00101). K.P.N. and A.M.G. are grateful for the access to the University of East Anglia NMR platforms as part of UEA Faculty of Science facilities. The access to The UK High-Field Solid-State NMR Facility (University of Warwick) had financial support from the PANACEA project that has received funding from the European Union's Horizon 2020 research and innovation programme under Grant Agreement No 101008500.

Funding

This research was funded by the Ministry of Science and Higher Education in Poland *via* grant number SUBK.D190.22.005.

References

Andersson, J., Rosenholm, J., Areva, S., Lindén, M., 2004. Influences of Material Characteristics on Ibuprofen Drug Loading and Release Profiles from Ordered Micro- and Mesoporous Silica Matrices. Chem. Mater. 16, 4160–4167. https://doi.org/10.1021/cm0401490

Ando, H., Ishii, M., Kayano, M., Ozawa, H., 1992. Effect of moisture on crystallization of theophylline in tablets. Drug Dev. Ind. Pharm. 18, 453–467. https://doi.org/10.3109/03639049209043863

Azaïs, T., Hartmeyer, G., Quignard, S., Laurent, G., Tourné-Péteilh, C., Devoisselle, J.-M., Babonneau, F., 2009. Solid-state NMR characterization of drug-model molecules encapsulated in MCM-41 silica. Pure Appl. Chem. 81, 1345–1355. https://doi.org/10.1351/PAC-CON-08-11-10

Azaïs, T., Tourné-Péteilh, C., Aussenac, F., Baccile, N., Coelho, C., Devoisselle, J.-M., Babonneau, F., 2006. Solid-State NMR Study of Ibuprofen Confined in MCM-41 Material. Chem. Mater. 18, 6382–6390.

https://doi.org/10.1021/cm061551c

Babonneau, F., Yeung, L., Steunou, N., Gervais, C., Ramila, A., Vallet-Regi, M., 2004. Solid State NMR Characterisation of Encapsulated Molecules in Mesoporous Silica. J. Sol-Gel Sci. Technol. 31, 219–223. https://doi.org/10.1023/B:JSST.0000047991.73840.8b

Badawy, S.I.F., Narang, A.S., LaMarche, K.R., Subramanian, G.A., Varia, S.A., Lin, J., Stevens, T., Shah, P.A., 2016. Integrated Application of Quality-by-Design Principles to Drug Product Development: A Case Study of Brivanib Alaninate Film–Coated Tablets. J. Pharm. Sci. 105, 168–181. https://doi.org/10.1016/j.xphs.2015.11.023

Bavnhøj, C.G., Knopp, M.M., Madsen, C.M., Löbmann, K., 2019. The role interplay between mesoporous silica pore volume and surface area and their effect on drug loading capacity. Int. J. Pharm. X 1, 100008. https://doi.org/10.1016/j.ijpx.2019.100008

Beiner, M., Rengarajan, G.T., Pankaj, S., Enke, D., Steinhart, M., Rengarajan, Pankaj, S., Enke, D., Steinhart, M., 2007. Manipulating the Crystalline State of Pharmaceuticals by Nanoconfinement. Nano Lett. 7, 1381–1385. https://doi.org/10.1021/nl0705081

Benedetto Tiz, D., Bagnoli, L., Rosati, O., Marini, F., Sancineto, L., Santi, C., 2022. New Halogen-Containing Drugs Approved by FDA in 2021: An Overview on Their Syntheses and Pharmaceutical Use. Molecules 27, 1643. https://doi.org/10.3390/molecules27051643

Cao, Y., Zhang, K., Gao, Z., Wang, J., Rohani, S., Gong, J., 2022. Preparation, Stabilization, and Dissolution Enhancement of Vortioxetine Hydrobromide Metastable Polymorphs in Silica Nanopores. Cryst. Growth Des. 22, 191–199. https://doi.org/10.1021/acs.cgd.1c00825

Cheng, S., McKenna, G.B., 2019. Nanoconfinement Effects on the Glass Transition and Crystallization Behaviors of Nifedipine. Mol. Pharm. 16, 856–866. https://doi.org/10.1021/acs.molpharmaceut.8b01172

Delle Piane, M., Corno, M., Pedone, A., Dovesi, R., Ugliengo, P., 2014a. Large-Scale B3LYP Simulations of Ibuprofen Adsorbed in MCM-41 Mesoporous Silica as Drug Delivery System. J. Phys. Chem. C 118, 26737–26749. https://doi.org/10.1021/jp507364h

Delle Piane, M., Vaccari, S., Corno, M., Ugliengo, P., 2014b. Silica-Based Materials as Drug Adsorbents: First Principle Investigation on the Role of Water Microsolvation on Ibuprofen Adsorption. J. Phys. Chem. A 118, 5801–5807. https://doi.org/10.1021/jp411173k

Dening, T.J., Taylor, L.S., 2018. Supersaturation Potential of Ordered Mesoporous Silica Delivery Systems. Part 1: Dissolution Performance and Drug Membrane Transport Rates. Mol. Pharm. 15, 3489–3501. https://doi.org/10.1021/acs.molpharmaceut.8b00488

Desai, S.R., Shaikh, M.M., Dharwadkar, S.R., 2002. Thermoanalytical study of polymorphic transformation in fluconazole drug. Thermochim. Acta 399, 81–89. https://doi.org/10.1016/S0040-6031(02)00451-3

Dolomanov, O.V., Bourhis, L.J., Gildea, R.J., Howard, J.A.K., Puschmann, H., 2009. OLEX2: a complete structure solution, refinement and analysis program. urn:issn:0021-8898 42, 339–341. https://doi.org/10.1107/S0021889808042726

Gackowski, M., Ruggiero-Mikołajczyk, M., Duraczyńska, D., Hinz, A., Bzowska, M., Szczepanowicz, K., 2021. The role of water in the confinement of ibuprofen in SBA-15. J. Mater. Chem. B 9, 7482–7491. https://doi.org/10.1039/D1TB01498F

Grün, M., Unger, K.K., Matsumoto, A., Tsutsumi, K., 1999. Novel pathways for the preparation of mesoporous MCM-41 materials: control of porosity and morphology. Microporous Mesoporous Mater. 27, 207–216. https://doi.org/10.1016/S1387-1811(98)00255-8

Grünberg, B., Emmler, T., Gedat, E., Shenderovich, I., Findenegg, G.H., Limbach, H.-H., Buntkowsky, G., 2004. Hydrogen Bonding of Water Confined in Mesoporous Silica MCM-41 and SBA-15 Studied by 1 H Solid-State NMR. Chem. - A Eur. J. 10, 5689–5696. https://doi.org/10.1002/chem.200400351

Ha, J.-M., Hamilton, B.D., Hillmyer, M.A., Ward, M.D., 2009. Phase Behavior and Polymorphism of Organic Crystals Confined within Nanoscale Chambers. Cryst. Growth Des. 9, 4766–4777. https://doi.org/10.1021/cg9006185

Ha, J.-M.M., Wolf, J.H., Hillmyer, M.A., Ward, M.D., 2004. Polymorph Selectivity under Nanoscopic Confinement. J. Am. Chem. Soc. 126, 3382–3383. https://doi.org/10.1021/ja049724r

Hamilton, B.D., Ha, J.-M., Hillmyer, M.A., Ward, M.D., 2012. Manipulating crystal growth and polymorphism by confinement in nanoscale crystallization chambers. Acc. Chem. Res. 45, 414–23. https://doi.org/10.1021/ar200147v

Han, Y., Lee, S.S., Ying, J.Y., 2007. Spherical siliceous mesocellular foam particles for high-speed size exclusion chromatography, in: Chemistry of Materials. American Chemical Society, pp. 829–832. https://doi.org/10.1016/S0167-2991(07)80447-2

Hasegawa, J., Hanano, M., Awazu, S., 1975. Decomposition of acetylsalicylic acid and its derivatives in solid state. Chem. Pharm. Bull. 23, 86–97. https://doi.org/10.1248/cpb.23.86

Horcajada, P., Rámila, A., Pérez-Pariente, J., Vallet-Regí, M., 2004. Influence of pore size of MCM-41 matrices on drug delivery rate. Microporous Mesoporous Mater. 68, 105–109. https://doi.org/10.1016/j.micromeso.2003.12.012

Jiang, Q., Ward, M.D., 2014. Crystallization under nanoscale confinement. Chem. Soc. Rev. 43, 2066–79. https://doi.org/10.1039/c3cs60234f

Kato, F., Otsuka, M., Matsuda, Y., 2006. Kinetic study of the transformation of mefenamic acid polymorphs in various solvents and under high humidity conditions. Int. J. Pharm. 321, 18–26. https://doi.org/10.1016/j.ijpharm.2006.04.020

Knight, A.W., Kalugin, N.G., Coker, E., Ilgen, A.G., 2019. Water properties under nano-scale confinement. Sci. Rep. 9, 8246. https://doi.org/10.1038/s41598-019-44651-z

Konno, H., Taylor, L.S., 2008. Ability of Different Polymers to Inhibit the Crystallization of Amorphous Felodipine in the Presence of Moisture. Pharm. Res. 25, 969–978. https://doi.org/10.1007/s11095-007-9331-3

Krueger, C., Thommes, M., Kleinebudde, P., 2014. Influence of storage condition on properties of MCC II-based pellets with theophylline-monohydrate. Eur. J. Pharm. Biopharm. 88, 483–491. https://doi.org/10.1016/j.ejpb.2014.06.006

Li, C., Wang, Yanqin, Guo, Yanglong, Liu, X., Guo, Yun, Zhang, Z., Wang, Yunsong, Lu, G., 2007. Synthesis of Highly Ordered, Extremely Hydrothermal stable SBA-15/Al-SBA-15 under the Assistance of Sodium Chloride. Chem. Mater. 19, 173–178. https://doi.org/10.1021/cm0619151

Lukens, W.W., Schmidt-Winkel, P., Zhao, D., Feng, J., Stucky, G.D., 1999. Evaluating Pore Sizes in Mesoporous Materials: A Simplified Standard Adsorption Method and a Simplified Broekhoff−de Boer Method. Langmuir 15, 5403–5409. https://doi.org/10.1021/la990209u

Malec, K., Monaco, S., Delso, I., Nestorowicz, J., Kozakiewicz-Latała, M., Karolewicz, B., Khimyak, Y.Z., Angulo, J., Nartowski, K.P., 2023. Unravelling the mechanisms of drugs partitioning phenomena in micellar systems via NMR spectroscopy. J. Colloid Interface Sci. 638, 135–148. https://doi.org/10.1016/j.jcis.2023.01.063

Mehta, M., Kothari, K., Ragoonanan, V., Suryanarayanan, R., 2016. Effect of Water on Molecular Mobility and Physical Stability of Amorphous Pharmaceuticals. Mol. Pharm. 13, 1339–1346.

https://doi.org/10.1021/acs.molpharmaceut.5b00950

Mellaerts, R., Roeffaers, M.B.J., Houthoofd, K., Van Speybroeck, M., De Cremer, G., Jammaer, J.A.G., Van den Mooter, G., Augustijns, P., Hofkens, J., Martens, J.A., 2011. Molecular organization of hydrophobic molecules and co-adsorbed water in SBA-15 ordered mesoporous silica material. Phys. Chem. Chem. Phys. 13, 2706–2713. https://doi.org/10.1039/C0CP01640C

Nartowski, K.P., Malhotra, D., Hawarden, L.E., Fábián, L., Khimyak, Y.Z., 2018. Nanocrystallization of Rare Tolbutamide Form V in Mesoporous MCM-41 Silica. Mol. Pharm. 15, 4926–4932. https://doi.org/10.1021/acs.molpharmaceut.8b00575

Nartowski, K.P., Malhotra, D., Hawarden, L.E., Sibik, J., Iuga, D., Zeitler, J.A., Fábián, L., Khimyak, Y.Z., 2016. 19 F NMR Spectroscopy as a Highly Sensitive Method for the Direct Monitoring of Confined Crystallization within Nanoporous Materials. Angew. Chemie Int. Ed. 55, 8904–8908. https://doi.org/10.1002/anie.201602936

Nartowski, K.P., Tedder, J., Braun, D.E., Fábián, L., Khimyak, Y.Z., 2015. Building solids inside nano-space: from confined amorphous through confined solvate to confined 'metastable' polymorph. Phys. Chem. Chem. Phys. 17, 24761–24773. https://doi.org/10.1039/C5CP03880D

Nowak, M., Dyba, A.J., Janczak, J., Morritt, A., Fábián, L., Karolewicz, B., Khimyak, Y.Z., Braun, D.E., Nartowski, K.P., 2022. Directing Crystallization Outcomes of Conformationally Flexible Molecules: Polymorphs, Solvates, and Desolvation Pathways of Fluconazole. Mol. Pharm. 19, 456–471. https://doi.org/10.1021/acs.molpharmaceut.1c00752

Nowak, M., Gajda, M., Baranowski, P., Szymczyk, P., Karolewicz, B., Nartowski, K.P., 2019. Stabilisation and Growth of Metastable Form II of Fluconazole in Amorphous Solid Dispersions. Pharmaceutics 12, 12. https://doi.org/10.3390/pharmaceutics12010012

Ohtake, S., Shalaev, E., 2013. Effect of Water on the Chemical Stability of Amorphous Pharmaceuticals: I. Small Molecules. J. Pharm. Sci. 102, 1139–1154. https://doi.org/10.1002/jps.23440

Otsuka, M., Ofusa, T., Matsuda, Y., 1999. Effect of environmental humidity on the transformation pathway of carbamazepine polymorphic modifications during grinding. Colloids Surfaces B Biointerfaces 13, 263–273. https://doi.org/10.1016/S0927-7765(99)00014-4

Paisana, M.C., Wahl, M.A., Pinto, J.F., 2016. Role of moisture on the physical stability of polymorphic olanzapine. Int. J. Pharm. 509, 135–148. https://doi.org/10.1016/j.ijpharm.2016.05.038

Pajzderska, A., Gonzalez, M.A., Mielcarek, J., Wąsicki, J., 2014. Water Behavior in MCM-41 As a Function of Pore Filling and Temperature Studied by NMR and Molecular Dynamics Simulations. J. Phys. Chem. C 118, 23701–23710. https://doi.org/10.1021/jp505490c

Paszun, S.K., Stanisz, B.J., 2013. Cilazapril decomposition kinetics and mechanism in the solid state versus stability of the other ester pro-drug angiotensin converting enzyme inhibitors. React. Kinet. Mech. Catal. 109, 285–300. https://doi.org/10.1007/s11144-013-0558-1

Ryoo, R., Jun, S., 1997. Improvement of Hydrothermal Stability of MCM-41 Using Salt Effects during the Crystallization Process. J. Phys. Chem. B 101, 317–320. https://doi.org/10.1021/jp962500d

Salas-Zúñiga, R., Mondragón-Vásquez, K., Alcalá-Alcalá, S., Lima, E., Höpfl, H., Herrera-Ruiz, D., Morales-Rojas, H., 2022. Nanoconfinement of a Pharmaceutical Cocrystal with Praziquantel in Mesoporous Silica: The Influence of the Solid Form on Dissolution Enhancement. Mol. Pharm. 19, 414–431. https://doi.org/10.1021/acs.molpharmaceut.1c00606

Skorupska, E., Jeziorna, A., Paluch, P., Potrzebowski, M.J., 2014. Ibuprofen in Mesopores of Mobil Crystalline Material 41 (MCM-41): A Deeper Understanding. Mol. Pharm. 11, 1512–1519.

https://doi.org/10.1021/mp400670f

Skorupska, E., Jeziorna, A., Potrzebowski, M.J., 2016. Thermal Solvent-Free Method of Loading of Pharmaceutical Cocrystals into the Pores of Silica Particles: A Case of Naproxen/Picolinamide Cocrystal. J. Phys. Chem. C 120, 13169–13180. https://doi.org/10.1021/acs.jpcc.6b05302

Skorupska, E., Paluch, P., Jeziorna, A., Potrzebowski, M.J., 2015. NMR Study of BA/FBA Cocrystal Confined Within Mesoporous Silica Nanoparticles Employing Thermal Solid Phase Transformation. J. Phys. Chem. C 119, 8652–8661. https://doi.org/10.1021/jp5123008

Trzeciak, K., Kaźmierski, S., Wielgus, E., Potrzebowski, M.J., 2020. DiSupLo - New extremely easy and efficient method for loading of active pharmaceutical ingredients into the pores of MCM-41 mesoporous silica particles. Microporous Mesoporous Mater. 308, 110506. https://doi.org/10.1016/j.micromeso.2020.110506

Veronica, N., Heng, P.W.S., Liew, C.V., 2022. Ensuring Product Stability – Choosing the Right Excipients. J. Pharm. Sci. 111, 2158–2171. https://doi.org/10.1016/j.xphs.2022.05.001

Vraníková, B., Niederquell, A., Šklubalová, Z., Kuentz, M., 2020. Relevance of the theoretical critical pore radius in mesoporous silica for fast crystallizing drugs. Int. J. Pharm. 591, 120019. https://doi.org/10.1016/j.ijpharm.2020.120019

Yerien, D.E., Bonesi, S., Postigo, A., 2016. Fluorination methods in drug discovery. Org. Biomol. Chem. 14, 8398–8427. https://doi.org/10.1039/C6OB00764C

Zhang, K., Fellah, N., López-Mejías, V., Ward, M.D., 2020. Polymorphic Phase Transformation Pathways under Nanoconfinement: Flufenamic Acid. Cryst. Growth Des. 20, 7098–7103. https://doi.org/10.1021/acs.cgd.0c01207

Zhao, D., Feng, J., Huo, Q., Melosh, N., Fredrickson, G.H., Chmelka, B.F., Stucky, G.D., 1998. Triblock Copolymer Syntheses of Mesoporous Silica with Periodic 50 to 300 Angstrom Pores. Science (80-.). 279, 548–552. https://doi.org/10.1126/science.279.5350.548

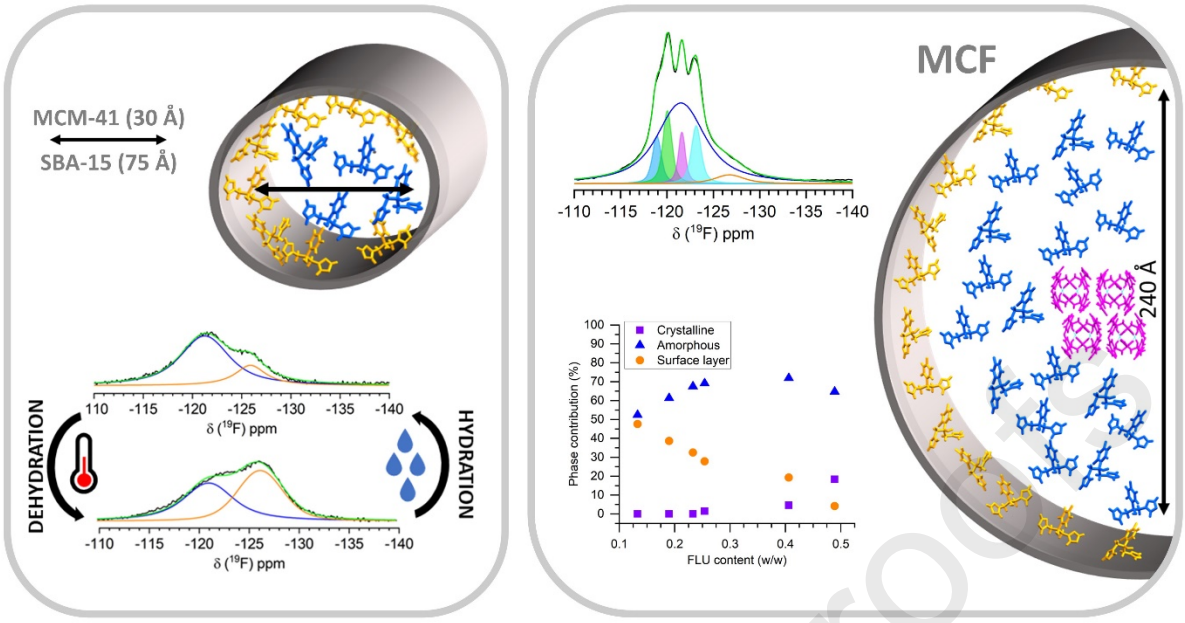

CRediT authorship contribution statement

Maciej Nowak: Conceptualization, Formal analysis, Investigation, Writing - Original Draft, Visualization, Funding acquisition. **Aleksandra J. Dyba:** Analysis, Investigation, Writing - Original Draft. **Anna M. Gołkowska:** Analysis, Investigation, Writing - Review & Editing. **Aleksandra Nieckarz:** Analysis, Investigation, Writing - Review & Editing. **Karolina Krajewska:** Analysis, Investigation, Writing - Review & Editing. **Katarzyna Malec:** Analysis, Investigation, Writing - Review & Editing. **Dinu Iuga:** Analysis, Investigation, Writing - Review & Editing. **Bożena Karolewicz:** Analysis, Investigation, Writing - Review & Editing. **Yaroslav Z. Khimyak:** Analysis, Conceptualization, Methodology, Investigation, Writing - Review & Editing, Funding acquisition. **Karol P. Nartowski:** Conceptualization, Methodology, Investigation, Writing - Review & Editing, Supervision, Funding acquisition.

Declaration of interests

☒ The authors declare that they have no known competing financial interests or personal relationships that could have appeared to influence the work reported in this paper.

☐ The authors declare the following financial interests/personal relationships which may be considered as potential competing interests: